

**Pulse compression in a silver gallium sulfide, mid-infrared,
synchronously pumped optical parametric oscillator**

R. Steven Kurti and Kenneth D. Singer

*Case Western Reserve University, Department of Physics,
Cleveland, OH 44106-7079*

Abstract

We present experiments and numerical modeling of optical pulse compression in a silver gallium sulfide synchronously pumped optical parametric oscillator. In the experiments, 10 ps pump pulses from a pulsed Nd:YAG laser interacted in the parametric oscillator to generate infrared output pulses as short as 500 fs, yielding over 20 fold compression. Parametric conversion and pulse compression were studied by numerical simulation of the nonlinear wave equations, and found to be in excellent agreement. The compression mechanism is related to group velocity walk-off in the nonlinear interaction. Dispersion measurements and simulations of pulse compression in the wavelength range of 2.5 – 4.0 μ m indicate that compression is inversely related to the signal-idler group velocity difference. Although compression requires group velocity walk-off between the pump and signal waves, the compression is most strongly controlled by the mismatch between the signal and idler group velocities.

OCIS 190.4970, 190.4410, 320.5520

Introduction

Parametric conversion of laser light by solid state materials is a common means of obtaining continuously tunable coherent radiation across a broad spectral range from the UV to the infrared. In addition to a broad spectral range, parametric conversion can be applied to many different types of lasers including pulsed lasers that generate tunable light pulses of femtosecond to nanosecond duration in optical parametric amplifiers (OPA's) and oscillators (OPO's) [1-7]. Along with each of these laser systems comes an ever widening array of materials [1-7].

Ultra short tunable pulse generation is most commonly performed by means of an optical parametric generator-amplifier (OPG-OPA) or simply OPA with an ultrafast pump laser. A disadvantage of OPA's is that they require a very intense pump source because of their one pass nature [8-10]. Typically, the pump source for an OPA is a relatively complex regenerative amplifier system [8], which requires high damage threshold nonlinear crystals. In the visible range, most of these systems use beta-barium borate (BBO) or lithium triborate (LBO) as the nonlinear optical crystal for the OPA [8] because of their excellent optical quality and high damage threshold. These materials, however, have limited applicability in the infrared region, where there are important applications in biomedical and chemical science and technology.

These biomedical and chemical applications require coherent light in the 1.0 – 10 μ m range. One nonlinear optical material that has good transmission in this region is silver gallium sulfide, AgGaS₂ (AGS) [11,12]. AGS has proven to be a desirable material for mid-infrared parametric conversion and difference frequency generation (DFG) since it is transparent from about 0.4 – 10 μ m [11]. Its main advantage is a relatively high value of its nonlinear optical coefficient, d , of about 12 pm/V for second harmonic generation. (BBO has a value of 2 pm/V).

[11]. Another attractive feature of AGS is that its absorption edge is at about 400nm, which means that it can be pumped at 1- μ m by a Nd:YAG without problems from two-photon absorption. Realizing femtosecond tunable pulses in AGS has been limited by the inability to pump directly with Ti:Sapphire lasers due to two-photon absorption and high average power. In addition, AGS has a relatively low damage threshold for nanosecond pulses[11] so that additional applications for short duration pulse are especially interesting.

Another route to ultrashort pulses that was originally suggested by Akhmanov et al. [13] involves compression due to group velocity mismatch. Interestingly, significant compression can occur when even in cases where dispersive broadening is a factor.[14] We and others have shown previously that SPOPO's can generate pulses on the order of hundreds of femtoseconds by compressing pump pulses from 1–10-ps in duration (either Q-switched or continuous wave) [15-21]. Such systems have been employed in spectroscopic studies.[22]

We and others have suggested models to explain the compression that occurs in SPOPO systems. It is generally believed that the compression is closely related to the group velocity mismatch between the pump and generated pulses[13,14,15,19,23] . Nonlinear conversion requires a temporal overlap of the pump and oscillating pulses in the nonlinear crystal, thus the amplification process is related to the overlap in time and space of the pump and oscillating OPO wave. Consequently, it has been suggested that a significant group velocity walk-off between the pump and oscillating wave would create a much shorter OPO output pulse relative to the input pump pulse.

In this paper we demonstrate pulse compression in AGS for generation of sub-picosecond pulses in the mid-infrared. We employ systematic experimental and numerical studies over a significant wavelength range to further elucidate the pulse compression mechanism in detuned

SPOPO's. Our experiments show a significant pulse compression in the 2.5 – 4.0 μm spectral region, and show excellent agreement with computer simulations of the nonlinear optical interaction. These studies over an extended wavelength range have demonstrated that the pulse compression depends not only on the group velocity walk-off between the pump and oscillating wave as previously discussed, but even more critically on the walk-off between the oscillating and non-oscillating wave.

Experimental Configuration

Our AGS SPOPO is pumped by an active-passive mode-locked, Q-switched Nd:YAG laser with passive negative feedback similar to those described in references 20 and 21. The laser operates at 1064nm with a repetition rate of 10 Hz and employs an oscillator-amplifier design. A saturable dye is used as the Q-switch, and an acousto-optic modulator mode-locks the system at about 120 MHz. The saturable dye also enables the mode-locking. A GaAs wafer oriented at Brewster's angle provides negative feedback to extend the pulse train and stabilize the pulse energy [24, 25,26]. The final output per lamp flash is a train of about 60 pulses separated by 8 ns (Figure 1) with each pulse having a FWHM of 10 ps and a maximum energy of 250 μJ . We are thus in the regime where dispersive pulse broadening is not a significant factor.[15]

Figure 2 shows our OPO configuration. This scheme is similar to a previous design[15, 27]. The OPO is based on two AGS crystals (Cleveland Crystals, Inc.) mounted such that they counter-rotate with respect to each other in order to compensate for transverse spatial walk-off between the pump and the generated waves [27]. Each crystal was cut for Type-I phase matching with the optic axis at 51.5° to the input surface normal with dimensions of 5mm x 7mm x 20mm with 20mm being along the propagation direction.

The OPO cavity is defined by two planar mirrors CM1 and CM2. CM1 is an aluminum mirror with a reflectivity of about 95%, while CM2 is a ZnSe wedge. The ZnSe was chosen because of its intrinsic reflection due to its large refractive index, which is between 2.43 and 2.45 over the wavelength range of interest. Thus, the reflectivity is about 17.5% and varies less than 1% over this wavelength range. The distance between CM1 and CM2 is set by minimizing the oscillation threshold as pump energy is decreased, with this position defining the zero for the cavity mismatch distance, dL . Mirror PSM1 steers the pump beam into the cavity and mirror PSM2 steers the pump out of the cavity. Both PSM1 and PSM2 are dielectric mirrors on CaF₂ substrates oriented at Brewster's angle to minimize reflective losses.

The cavity is aligned such that the beams are slightly non-collinear. In this way, the oscillating and non-oscillating beams can easily be spatially distinguished. The non-oscillating wave in the OPO cavity is directed out of the cavity by means of an aluminum mirror while the oscillating wave exits the cavity through the ZnSe wedge. This geometry reduces the effects of unwanted satellite pulses in the cavity.

Measurements of the OPO output temporal characteristics are performed with a second harmonic, non-collinear phase matching intensity autocorrelator. In order to access the entire wavelength range, two different second-harmonic crystals and three different detectors were used in the autocorrelator. For shorter wavelengths a 1-mm LiIO₃ crystal is employed while at longer wavelengths a 1-mm AGS crystal is used. To increase the signal to noise, detectors were chosen such that the band gap of each detector was between the energies of the fundamental and the second harmonic of the OPO output.

Experimental Procedure and Results

Since we are measuring the pulse compression variation with wavelength, we require a parameter that enables us to compare the incident energy dependence of pulse compression at various wavelengths due to differences in reflection as the crystal is angle tuned. Since, incident energy is a key parameter in the compression of pulses [15], we normalize all of our energy values to the energy of the pump at the SPOPO oscillation threshold value. Therefore, we define a dimensionless energy parameter,

$$EN = \frac{E_{pump}}{E_{pump@threshold}}. \quad (1.1)$$

Since AGS has a relatively low damage threshold, EN was limited to 4 in most cases. However for crystal tuning angles far from normal incidence, the pumping energy must be increased to offset the higher reflection losses incurred at higher angles. Thus, far from normal incidence the experimentally accessible values of EN decreased.

For purposes of comparison, autocorrelations were fit to a Gaussian. When satellite pulses were observed[15], only the central peak was fit. Examples of the autocorrelations and their corresponding fits appear in Figure 3. We define a compression parameter as the following ratio,

$$Compression = \frac{FWHM_{pump}}{FWHM_{OPO\ output}}, \quad (1.2)$$

where the full-width half-maxima (FWHM) are determined by fits to a Gaussian in the case of our measurements. We found that at compressions greater than about 10, the quality of the compressed pulses deteriorated significantly, as suggested by Figures 3a and 3b.[21]

As mentioned previously, the zero point for dL is defined as the value for which the SPOPO has the lowest threshold of oscillation. We are most interested in the values of dL for which compression is maximum. As shown in Figure 4 there is a maximum in the compression as a function of dL for each wavelength. It should be noted that the value of dL , for which compression is maximum, changes for different energies and wavelengths. Also maximum compression occurs only for positive values of dL .

For each value of energy and crystal phase matching angle, there are four possible measurements that are related to the two generated wavelengths. Thus when specifying a temporal measurement at a given energy and phase matching angle, the wavelength and oscillation state must be specified. The four measurements are: (1) long wavelength oscillating and measured, (2) short wavelength oscillating and measured, (3) long wavelength oscillating and short wavelength measured, and (4) short wavelength oscillating and long wavelength measured. We found that compression is observed in all four cases to varying degrees. However, significant compression (compression > 10) is only observed in the oscillating wave when the longer of the two wavelengths is oscillating. For the remainder of this paper, only case (1) will be considered.

Figure 5 shows a plot of maximum compression as a function of EN for each wavelength sampled. Compression is found to monotonically increase with energy and simulations indicate that it tends to saturate near degeneracy and for high values of EN . The highest value of compression we observed was a little more than 20 at $EN = 2$ and a wavelength of 2476 nm.

Figure 6 shows data plotted with compression as a function of wavelength for each value of EN.

In this plot the compression decays rapidly as a function of wavelength for each value of EN.

These trends will be further discussed in later sections.

Theory and Simulations

To understand the experimental data, we carried out numerical simulation of the nonlinear optical process using the SNLO simulation package (see reference 28). The SPOPO part of the software was specially modified by the author so that batch processing could be performed. The solution engine for the SPOPO portion of the SNLO software integrates the following set of coupled equations using a Runge-Kutta method:

$$\left(\frac{\partial}{\partial z} + \frac{1}{v_s} \frac{\partial}{\partial t} + i\alpha_s \frac{\partial^2}{\partial t^2} \right) \varepsilon_s(t, z) = \frac{i\omega_s d_{eff}}{n_s c} \varepsilon_p(t, z) \varepsilon_i^*(t, z) e^{i\Delta k z} \equiv P_s(t, z) \quad (1.3)$$

$$\left(\frac{\partial}{\partial z} + \frac{1}{v_i} \frac{\partial}{\partial t} + i\alpha_i \frac{\partial^2}{\partial t^2} \right) \varepsilon_i(t, z) = \frac{i\omega_i d_{eff}}{n_i c} \varepsilon_p(t, z) \varepsilon_s^*(t, z) e^{i\Delta k z} \equiv P_i(t, z) \quad (1.4)$$

$$\left(\frac{\partial}{\partial z} + \frac{1}{v_p} \frac{\partial}{\partial t} + i\alpha_p \frac{\partial^2}{\partial t^2} \right) \varepsilon_p(t, z) = \frac{i\omega_p d_{eff}}{n_p c} \varepsilon_i(t, z) \varepsilon_s(t, z) e^{-i\Delta k z} \equiv P_p(t, z) \quad (1.5)$$

where Δk is the phase velocity mismatch between the three waves and the interacting photon

frequencies satisfy $\omega_p = \omega_s + \omega_i$. The fields of each wave are defined as

$$E_j(t, z) = \frac{1}{2} \left\{ \varepsilon_j(t, z) e^{-i(\omega_j t - k_j z)} + \varepsilon_j^*(t, z) e^{i(\omega_j t - k_j z)} \right\} \quad (1.6)$$

where j can be s, i, or p corresponding to the signal, idler, and pump waves. The group velocity of each wave is denoted as v_j where j can again be s, i, or p. The group velocity is defined as $v_g = \partial\omega / \partial k$. The effective nonlinear optical coefficient is d_{eff} . For the purpose of these simulations the signal wave is always considered to be the wave optimized for oscillation in the OPO cavity. The group velocity dispersion enters the simulation by means of the third term in which $\alpha_j = (1/2)(\partial^2 k_j / \partial \omega_j^2)$. Additional information about the methods used in the SNLO software is available in reference 29.

We simulated the autocorrelations in order to compare directly to the data. The simulation generated for each of the three interacting waves, an array for the intensity and an array for the phase. In order to closely simulate our experimental setup, each simulation run consists of 60 iterations through the cavity corresponding to the average of 60 pulses of our pump source. To save calculation time we only sampled the output from the simulation every fifth iteration.

In the experiment, the dynamic progression of the nonlinear interaction is detected as each of the approximately 60 pulses in the train proceeds. Thus, the entire dynamic progression is detected and integrated over the pulse train by the detector and boxcar integration. One then detects not only the resulting compressed pulse, but the average of the compression dynamic. (This is in contrast to the detection from a CW mode-locked laser where the initial dynamic is transient.) This was simulated numerically by integrating over the results of each pass in the SPOPO simulation. The final output of our analysis is an autocorrelation plot averaged over the dynamics behavior of the pulses in the train. Once an autocorrelation is obtained, the FWHM is measured and normalized by the pump FWHM to arrive at the compression.

The threshold of oscillation for the simulation was defined as the smallest energy with appropriate dL such that the peak signal and idler wave intensities reached a significant fraction (about 30%) of the peak pump intensity by iteration number 60. Values for the energies were then chosen similarly to the energies chosen for the experiments using the dimensionless energy parameter EN.

As with the experiments, it is most useful to compare maximum compression as a function of EN and wavelength. Figure 5 shows a plot of maximum compression as a function of EN for both the experiments and the simulation. The compression is again a monotonically increasing function of energy as is the experiment. Excellent agreement between experiment and simulation with no adjustable parameters is observed.

Figure 6 shows again the same data with compression as a function of wavelength. We note from both Figures 5 and 6 that there is excellent agreement between theory and simulation without adjustment of parameters. Thus it is reasonable to employ the simulation to deduce information that is not necessarily available from the experiments such as output intensity, phase of the fields, and the dependence of compression on individual input parameters.

In order to understand the dispersion of the compression shown in Figure 6, we examine the simulations and the physical mechanism behind them. Previous work on the subject of pulse compression in OPO's has indicated that this phenomenon arises from the difference between the group velocities of the pump and oscillating wave [15]. This difference in group velocities we will call group velocity mismatch (GVM) defined as

$$GVM_{jk} = \frac{1}{c} (V_g^j - V_g^k) \quad (1.7)$$

where V_g^j refers to the group velocity of wave j (j and k can be p for pump, i for idler, or s for signal). In this picture, higher values of GVM_{sp} lead to limited temporal overlap between the pump and signal waves [15] and consequential nonlinear interactions. Plots of GVM_{sp} and GVM_{ip} for AGS appear in Figures 7a and 7b. Since Figure 6 indicates a decrease in compression in the wavelength range beyond the degeneracy point of the OPO at 2.128 μm up to 4.0 μm , it seems that compression does not increase with either type of group velocity mismatch.

In order to understand the factors that contribute most strongly to compression, a thorough study of the simulation parameter space was conducted. The contributions of the various parameters (wavelength, phase velocity, group velocity, group velocity dispersion, linear and nonlinear absorption, nonlinear index, pump pulse energy, and dL) were investigated by varying each one in turn. Except for the group velocity differences, pulse energy and dL, the simulations were relatively insensitive to even orders of magnitude variation of the other parameters. It was observed that both the threshold and compression depended strongly on group velocity mismatches. There are three group velocities mismatches to consider: that of the pump and signal (oscillating) GVM_{sp} , the signal and idler (nonoscillating) GVM_{is} , and the pump and idler GVM_{ip} . Each of these combinations was examined, but we found that GVM_{ip} did not significantly affect compression.

It was found that group velocity mismatches or walk-offs GVM_{sp} and GVM_{is} were most significant. We examined the effects of these parameters by hypothetically varying the group velocities within the range of the dispersion of AGS in this wavelength range, keeping other parameters constant. A summary of the results appears in Figure 8. This three dimensional plot shows maximum compression on the vertical axis, GVM_{is} on the left axis, and GVM_{sp} on the

right axis. From this plot it is clear that as GVM_{is} decreases maximum compression increases. It can also be seen that increasing GVM_{sp} causes maximum compression to increase, although compression is not nearly as sensitive to GVM_{sp} as it is to GVM_{is} . To elucidate the scale of compression changes with respect to GVM Figure 9a shows a plot of GVM_{sp} at $GVM_{is} = 0.006$ while Figure 9b shows a plot of GVM_{is} at $GVM_{sp} = 0.014$. Comparing the average slope of these two curves indicates that compression is more than an order of magnitude more sensitive to GVM_{is} than to GVM_{sp} . Thus we conclude that the group velocity difference between the idler and signal is a most important factor affecting compression.

Discussion

Our results indicate that compression requires an efficient, but time-limited interaction between the various pulses. The increase in compression with increasing EN and decreasing GVM_{is} corresponds to enhanced nonlinear optical interaction. Minimum GVM_{is} provides for maximum nonlinear conversion during the compression interaction, that is, maximum overlap between all three pulses during compression. The finite GVM_{ps} required for compression arises from a time-limited interaction between the previously generated pulse circulating in the cavity and the most recent pump pulse.

From these studies, we conclude that there are two main methods for achieving compression. First, our results agree with previous results that suggest that large group velocity differences between the pump and signal waves are necessary for compression [15]. Second, our results additionally confirm that increasing the energy of the nonlinear interaction (synonymous with significant overlap between the idler and signal waves) increases the compression because of the nonlinear nature of the amplification of pulses in a SPOPO.

On a practical note, it has previously been suggested that it should be possible to achieve pulses under 100 femtoseconds by using a pump source that with a 1 ps pulse instead of a 10 ps pulse [15]. Also while our experiments were only able to extend from 2.5 – 4.0 μm , AGS has good transparency characteristics out as far as 9.5 μm . Some of our additional simulations have also shown that significant compression occurs all the way out to 9 μm . Thus a properly pumped and tuned AGS SPOPO could be used to generate femtosecond radiation across a broad range in the mid-infrared.

Conclusion

We demonstrated 20 fold pulse compression in a synchronously pumped optical parametric oscillator based on an AGS. The shortest pulse measured was about 500 femtoseconds. Pulse compression was measured in the 2.5 – 4.0 μm range and simulated to continue out to the transparency limit near 9.0 μm . It was found that compression is strongest when the the group velocity mismatch between the idler and signal is minimum. This implies that compression is strongest near degeneracy, and may limit the magnitude of pulse compression for generating short duration pulses at wavelengths far from degeneracy.

We simulated our experimental results using SNLO software. While it has previously been shown that the pulse compression is a result of a group velocity mismatch between the pump and the oscillating wave, our simulations have demonstrated that the group velocity difference between the oscillating and non-oscillating waves of the SPOPO plays an important role as well.

We have shown that AGS can successfully produce femtosecond radiation across a broad spectrum in the mid-infrared, but may be ultimately limited at wavelengths far from degeneracy due to the strong dependence on the signal-idler walk-off. Applicability to the compression

scheme discussed here will depend on the ability to form cleaner pulses such as might be attained with shorter duration pump pulses, and/or in CW mode-locked systems

Acknowledgments

We would like to thank Cleveland Crystals, Inc. for the loan and maintenance of the AgGaS₂ crystals used in this work, and to Robert Eckardt and Gary Catella of Cleveland Crystals for helpful discussions. We are also grateful to Dr. Arlee Smith for helpful discussion, and for modifying his simulation package for our needs. We would also like to acknowledge helpful comments by John Khaydarov of Continuum, Inc. Finally, R. S. Kurti would like to acknowledge support from the Department of Education via his GAANN graduate fellowship.

References

1. V. A. Dyakov, V. I. Pryalkin, A. I. Kholodnykh, "Optical parametric oscillator utilizing potassium niobate crystal pumped by the 2nd garnet laser harmonic," *Kvantovaya Elektron+* **8**, 715-721 (1981).
2. R. C. Eckhardt, Y. X. Fan, R. L. Byer, et al, "Broadly tunable infrared parametric oscillator using AgGaSe₂," *Appl. Phys. Lett.* **49**, 608-610 (1986).
3. L. K. Cheng, W. R. Bosenberg, C. L. Tang, "Broadly tunable optical parametric oscillation in beta-BaB₂O₄," *Appl. Phys. Lett.* **53**, 175-177 (1988).
4. K. Kato, "Parametric oscillation in LiB₃O₅ pumped at 0.532 μ m," *IEEE J. Quant. Elect.* **26**, 2043-2045 (1990).
5. D. Josse, S. X. Dou, J. Zyss, P. Andreazza, and A. Périgaud, "Near-infrared optical parametric oscillation in a N-(4-nitrophenyl)-L-prolinol molecular crystal," *Appl. Phys. Lett.* **61**, 121-123 (1992).
6. V. Pruneri, J. Webjörn, P. St. J. Russell, and D. C. Hanna, "532nm pumped optical parametric oscillator in bulk periodically poled lithium-niobate," *Appl. Phys. Lett.* **67**, 2126-2128 (1995).
7. T. H. Allik, S. Chandra, D. M. Rines, P. G. Schunemann, J. A. Hutchinson, and R. Utano, "Tunable 7-12- μ m optical parametric oscillator using a Cr,Er:YSGG laser to pump CdSe and ZnGeP₂ crystals," *Opt. Lett.* **22**, 597-599 (1997).
8. R. L. Sutherland, Handbook of Nonlinear Optics, second ed. (Merzel Dekker, New York, 2003).

9. R. Danielius, A. Piskarskas, A. Stabinis, G. P. Banfi, P. Di Trapani, and R. Righini, "Traveling-wave parametric generation of widely tunable, highly coherent femtosecond light pulses," *J. Opt. Soc. Am. B* **10**, 2222 (1993).
10. F. Seifert, V. Petrov, and F. Noack, "Sub-100-fs optical parametric generator pumped by a high-repetition-rate Ti:Sapphire regenerative amplifier system," *Opt. Lett.* **19**, 837 (1994).
11. V. G. Dmitriev, G. G. Gurdzadyan, D. N. Nikogosyan, *Handbook of Nonlinear Optical Materials*, Springer-Verlag, 1991.
12. A. Douillet, J.J. Zondy, A. Yelisseyev, S. Lobanov, and L. Isaenko L, "Toward a 3 : 1 frequency divider based on parametric oscillation using AgGaS₂ and PPLN crystals," *IEEE Trans. Ultrason., Ferroelect, and Freq. Control* **47**, 1127-1133 (2000).
13. S.A. Akhmanov, A.S. Chirkin, K.N. Drabovich, A.I. Kovrigin, R.V. Khokhlov, and A.P. Sukhorukov, "Nonstationary nonlinear optical effects and ultrashort light pulse formation," *IEEE J. Quant. Electron.* **QE-4**, 598 (1968).
14. V. Vasilyauskas, A. Piskarskas, and A. Stabinis, "Self-compression of femtosecond light pulses in media with a quadratic nonlinearity under conditions of group velocity mismatch," *Sov. J. Quant. Electron.* **18**, 518 (1988).
15. J. D. Khaydarov, J. H. Andrews, K. D. Singer, "Pulse-compression mechanism in a synchronously pumped parametric oscillator," *J. Opt. Soc. Am. B* **12**, 2199-2208 (1995).
16. E. Gaizauskas, R. Grigonis, and V. Sirutkaitis, "Self- and cross-modulation effects in a synchronously pumped parametric oscillator," *J. Opt. Soc. Am. B* **19**, 2957-2966 (2002).

17. A. Angesi, A. Lucca, G. Reali, and A. Tomaselli, "All-solid-state high-repetition-rate optical source tunable in wavelength and in pulse duration," *J. Opt. Soc. Am. B* **18**, 286-290 (2001).
18. J. D. Kafka, M. L. Watts, and J. W. Pieterse, "Synchronously pumped optical parametric oscillators with LiB₃O₅," *J. Opt. Soc. Am. B* **12**, 2147-2157 (1995).
19. L. Lefort, K. Puech, S. D. Butterworth, Y. P. Svirko, and D. C. Hanna, "Generation of femtosecond pulses from order-of-magnitude pulse compression in a synchronously pumped optical parametric oscillator based on periodically poled lithium niobate," *Opt. Lett.* **24**, 28-30 (1999).
20. J.D.V. Khaydarov, J.H. Andrews, and K.D. Singer, "Pulse compression in a synchronously pumped optical parametric oscillator from group-velocity mismatch," *Opt. Lett.* **19**, 831-833 (1994).
21. J.D.V. Khaydarov, J.H. Andrews, and K.D. Singer, "20-fold pulse compression in a synchronously pumped optical parametric oscillator," *Appl. Phys. Lett.* **65**, 1614-1616 (1994).
22. R. Laenen, K. Simeonidis, and A. Laubereau, "Generation of sub-ps IR pulses via parametric processes and application to transient spectroscopy of molecules," *Laser Phys.* **9** 234-238 (1999).
23. E. Ibragimov, A. A. Struthers, D. J. Kaup, J. D. Khaydarov, and K. D. Singer, "Three-wave interaction solitons in optical parametric amplification," *Phys. Rev. E* **59**, 6122-6137 (1999).
24. A. Agnesi, A. Del Corno, P. Di Trapani, M. Fogliani, G. C. Reali, J.-C. Diels, C. Y. Yeh, X. M. Zhao, and V. Kubeck, "Generation of extended pulse trains of minimum

- duration by passive negative feedback applied to solid-state Q-switched lasers,” *IEEE J. Quantum Electron.* **28**, 710 (1992).
25. A. Agnesi, G. C. Reali, V. Kubeck, S. Kumazaki, Y. Takagi, and K. Yoshihara, “ β -Barium borate and lithium triborate picosecond parametric oscillators pumped by a frequency-tripled passive negative-feedback mode-locked Nd:YAG laser,” *J. Opt. Soc. Am. B* **10**, 2211 (1993).
 26. A. Agnesi, A. Del Corno, P. Di Trapani, M. Fogliani, G.G. Reali, J.-C. Diels, C.Y. Yeh, X.M. Zhao, and V. Kubecek,” Generation of extended pulse trains of minimum duration by passive negative feedback applied to solid-state Q-switched lasers,” *IEEE J. Quant. Electron.* **28**, 710 (1992).
 27. W. R. Bosenberg, W. S. Pelouch, and C. L. Tang, “High-efficiency and narrow-linewidth operation of a two-crystal β -BaB₂O₄ optical parametric oscillator,” *Appl. Phys. Lett.* **55**, 1952 (1989).
 28. A. V. Smith, R. J. Gher, M. S. Bowers, “Numerical models of broad-bandwidth nanosecond optical parametric oscillators,” *J. Opt. Soc. Am. B* **16**, 609-619 (1999).
 29. A. V. Smith, “SNLO Version 36,” <http://www.sandia.gov/imrl/X1118/xxtal.htm>.

List of Figures

Figure 1. The output train of our Nd:YAG laser.

Figure 2. Our AGS SPOPO. Cavity mirrors CM1, CM2. Pump steering mirrors PSM1, PSM2.

Figure 3. Autocorrelations of the pump and a compressed pulse from the OPO along with the corresponding fitting curves: (a) 1.2 ps pulses, compression of 6.5 and (b) 580 fs pulse, compression of 13.2.

Figure 4. Compression as a function of dL.

Figure 5. Maximum compression as a function of EN for each wavelength, both simulations (sim) and data. Triangles and solid line, 2476nm; circles and dotted line, 3016nm; squares and dashed line, 4000nm.

Figure 6. Maximum compression as a function of wavelength for each value of EN, both simulations (sim) and data. Circles and solid line, EN=1.5; triangles and dotted line, EN=2.

Figure 7. Group velocity mismatch (GVM) as a function of wavelength in microns: (a) GVM_{sp} and (b) GVM_{is} .

Figure 8. Maximum compression as a function of GVM_{is} and GVM_{sp} .

Figure 9. Maximum compression as a function of (a) GVM_{sp} and (b) GVM_{is} .

R.S. Kurti and K.D. Singer

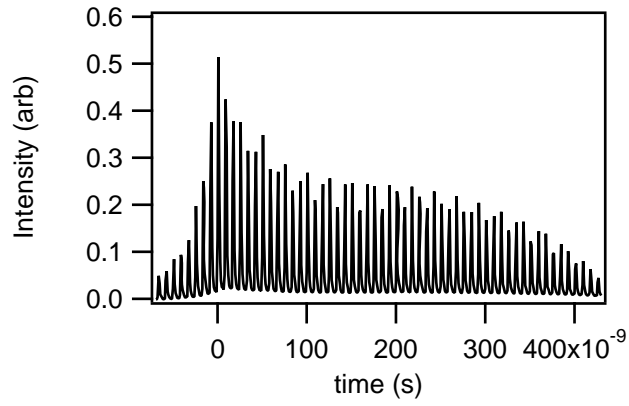


Figure 1: The output train of our Nd:YAG laser.

R.S. Kurti and K.D. Singer

“Pulse compression in a silver gallium sulfide, mid-infrared, synchronously pumped optical parametric oscillator”

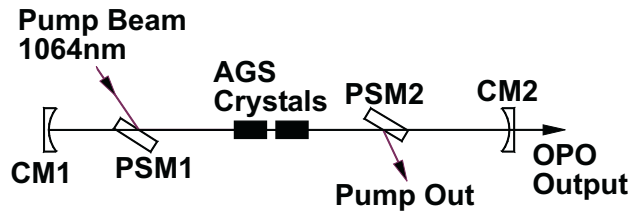


Figure 2: Our AGS SPOPO. Cavity mirrors CM1, CM2. Pump steering mirrors PSM1, PSM2.
R.S. Kurti and K.D. Singer
“Pulse compression in a silver gallium sulfide, mid-infrared, synchronously pumped optical parametric oscillator”

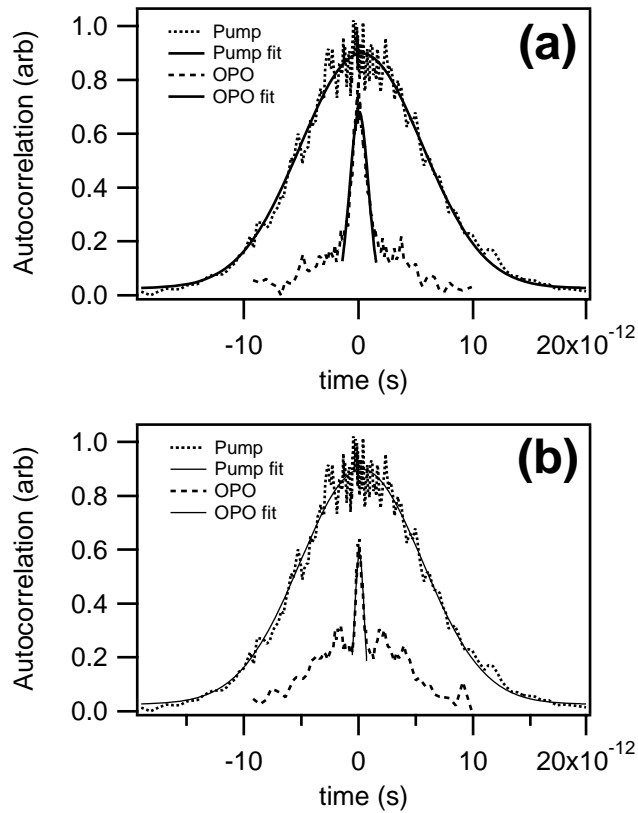


Figure 3: Autocorrelations of the pump and a compressed pulse from the OPO along with the corresponding fitting curves: (a) 1.2 ps pulses, compression of 6.5 and (b) 580 fs pulse, compression of 13.2.

R.S. Kurti and K.D. Singer

“Pulse compression in a silver gallium sulfide, mid-infrared, synchronously pumped optical parametric oscillator”

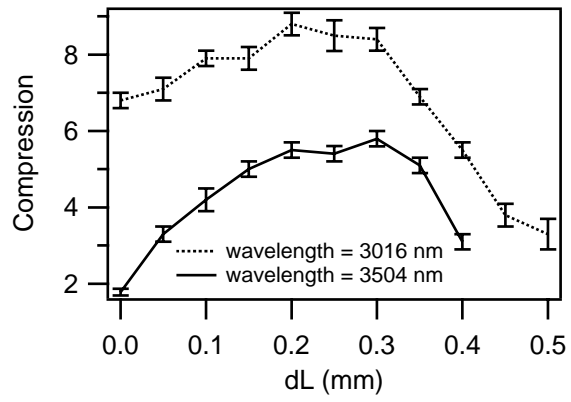


Figure 4: Compression as a function of dL.

R.S. Kurti and K.D. Singer

“Pulse compression in a silver gallium sulfide, mid-infrared, synchronously pumped optical parametric oscillator”

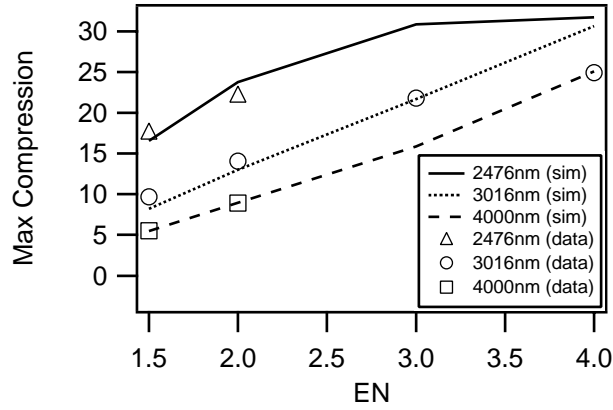


Figure 5: Maximum compression as a function of EN for each wavelength, both simulations (sim) and data. Triangles and solid line, 2476nm; circles and dotted line, 3016nm; squares and dashed line, 4000nm.

R.S. Kurti and K.D. Singer

“Pulse compression in a silver gallium sulfide, mid-infrared, synchronously pumped optical parametric oscillator”

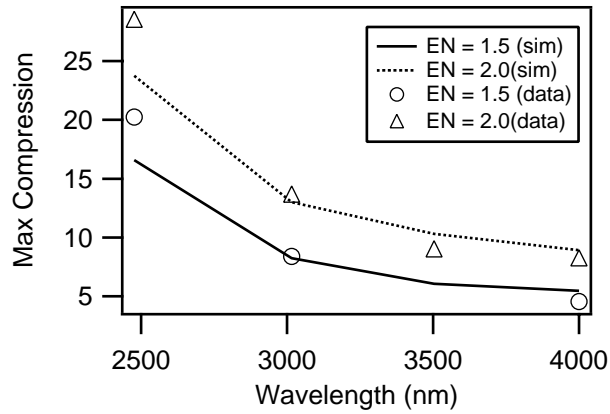


Figure 6: Maximum compression as a function of wavelength for each value of EN, both simulations (sim) and data. Circles and solid line, EN=1.5; triangles and dotted line, EN=2.

R.S. Kurti and K.D. Singer

“Pulse compression in a silver gallium sulfide, mid-infrared, synchronously pumped optical parametric oscillator”

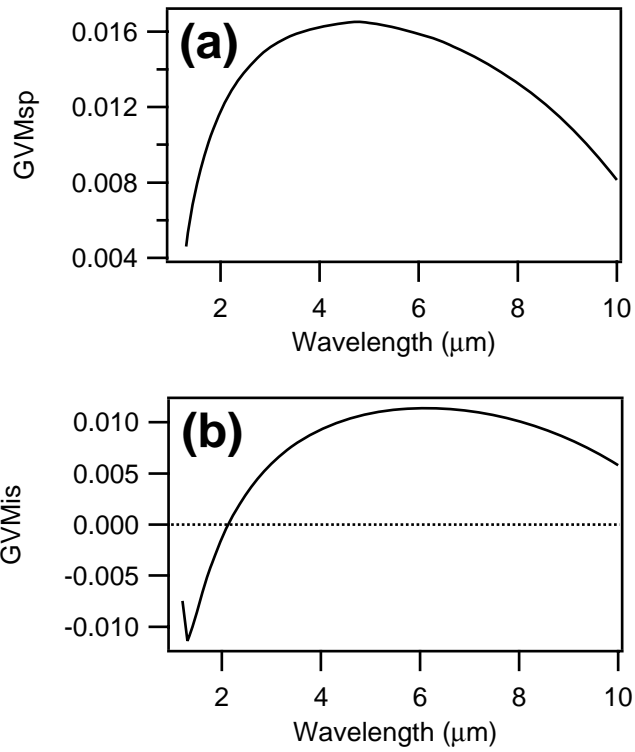


Figure 7: Group velocity mismatch (GVM) as a function of wavelength in microns: (a) GVM_{sp} and (b) GVM_{is} .

R.S. Kurti and K.D. Singer

“Pulse compression in a silver gallium sulfide, mid-infrared, synchronously pumped optical parametric oscillator”

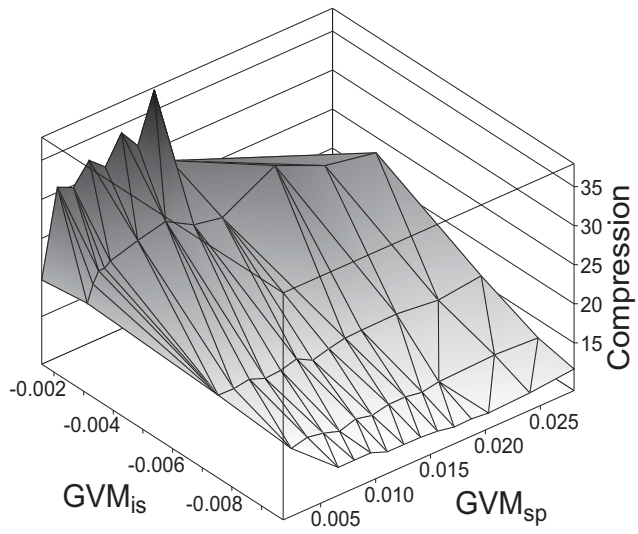


Figure 8: Maximum compression as a function of GVM_{is} and GVM_{sp} for $EN=2$.
 R.S. Kurti and K.D. Singer
 “Pulse compression in a silver gallium sulfide, mid-infrared, synchronously pumped optical parametric oscillator”

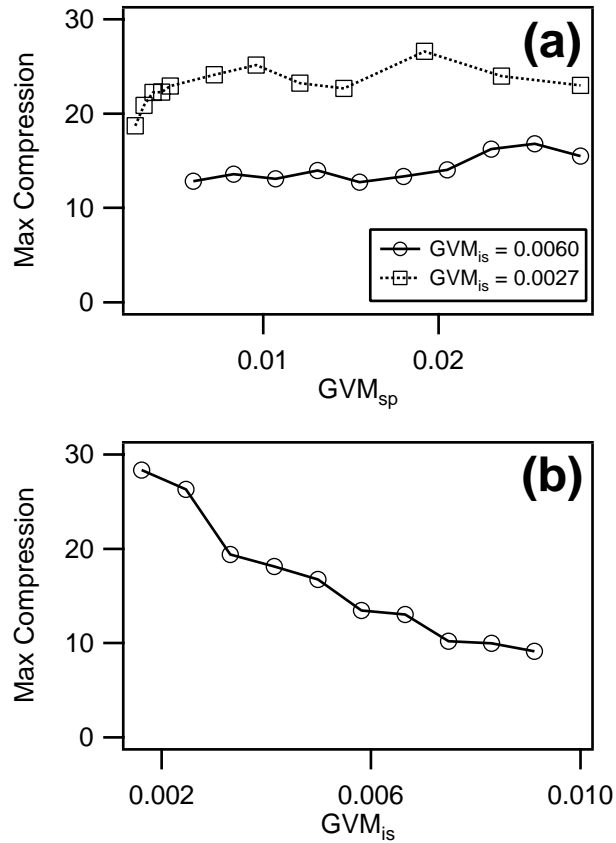


Figure 9: Maximum compression as a function of (a) GVM_{sp} and (b) GVM_{is} for EN=2.

R.S. Kurti and K.D. Singer

“Pulse compression in a silver gallium sulfide, mid-infrared, synchronously pumped optical parametric oscillator”